


## Article

# Enhanced Sensitivity of a Resistive Pressure Sensor Based on a PEDOT:PSS Thin Film on PDMS with a Random-Height Micropyramid Structure

Sungyong Kim <sup>1</sup>  and Dae Yu Kim <sup>1,2,3,\*</sup>

<sup>1</sup> Department of Electrical and Computer Engineering, College of Engineering, Inha University, Incheon 22212, Republic of Korea; ksy@inha.edu

<sup>2</sup> Center for Sensor Systems, Inha University, Incheon 22212, Republic of Korea

<sup>3</sup> Inha Research Institute for Aerospace Medicine, Inha University, Incheon 22212, Korea

\* Correspondence: dyukim@inha.ac.kr; Tel.: +82-032-860-7394

**Abstract:** The use of flexible pressure sensors has become increasingly widespread in a variety of applications, including wearable electronics and electronic skin. These sensors need to exhibit high sensitivity, wide detection limits, a fast response time, a linear response, and mechanical stability. In this study, we demonstrate a resistive pressure sensor based on randomly arranged micropyramid polydimethylsiloxane (PDMS) with a conductive poly(3,4-ethylenedioxythiophene): polystyrenesulfonate (PEDOT:PSS) thin film with a sensitivity of  $391 \text{ kPa}^{-1}$ , a response time of 52.91 ms, a recovery time of 4.38 ms, and a limit of detection (LOD) of 0.35 kPa. Electrodes are then connected to a pair of the proposed resistive pressure sensors that face each other to fabricate a pressure sensing device. We examine various characteristics of the fabricated device, including the changes observed when applying loads ranging from 0 to 2.58 kPa. The proposed sensor exhibits high sensitivity and a rapid response time.

**Keywords:** piezoresistive sensor; resistive pressure sensor; PDMS/PEDOT:PSS; micropyramid structure



**Citation:** Kim, S.; Kim, D.Y. Enhanced Sensitivity of a Resistive Pressure Sensor Based on a PEDOT:PSS Thin Film on PDMS with a Random-Height Micropyramid Structure.

*Micromachines* **2024**, *15*, 1110.  
<https://doi.org/10.3390/mi15091110>

Academic Editor: Ai-Qun Liu

Received: 13 July 2024

Revised: 27 August 2024

Accepted: 28 August 2024

Published: 31 August 2024



**Copyright:** © 2024 by the authors. Licensee MDPI, Basel, Switzerland. This article is an open access article distributed under the terms and conditions of the Creative Commons Attribution (CC BY) license (<https://creativecommons.org/licenses/by/4.0/>).

## 1. Introduction

Flexible pressure sensors are becoming increasingly common in wearable electronics [1,2], electronic skin [3,4], electronic devices [5], and robotics [6,7]. Pressure sensors measure pressure signals, which are defined as the ratio of a force to the area on which the force acts [8], and can be classified as piezoresistive [9,10], capacitive [11,12], or piezoelectric [13,14] depending on their sensing mechanism. Piezoresistive pressure sensors have received particular attention for a number of key advantages, such as their more straightforward manufacturing process, relatively high sensitivity, wide sensing range, and excellent anti-interference properties [15]. They can also be manufactured with a small size and consist of elastic conductive materials, allowing for a more flexible device structure and a wider deformation range [16].

Nevertheless, piezoresistive pressure sensors are expensive, cannot be mass-produced, and often exhibit poor stability [17,18]. In addition, there has been a drive to further increase the sensitivity of flexible pressure sensors so that they can be incorporated into sensing devices for the detection of other external signals, such as temperature and humidity [19,20]. To improve the sensitivity, it is important to tune the microstructure of the dielectric layer, which increases the manufacturing complexity of the sensor. As such, there remain a number of challenges to overcome to simplify this technology and increase its sensitivity.

The operational basis of piezoresistive pressure sensors is their ability to detect changes in resistance in response to external pressure stimuli, known as the piezoresistive effect. In this process, resistance  $R$  is expressed as

$$R = \rho \frac{l}{s} \quad (1)$$

where  $\rho$  is the specific resistance of the material,  $l$  is its total length, and  $s$  is the cross-sectional area. The resistance of the material thus changes with  $l$  and  $s$  as it deforms.

Piezoresistive pressure sensors are typically fabricated with active materials positioned between two electrodes that are vertically aligned [21,22]. For decades, tremendous efforts have been made to improve sensor performance with bi- and trilayer microstructures [23,24], deformable electrodes [25,26], and novel durable materials [27]. The bi- and trilayer microstructures, consisting of flexible microstructured substrates as well as conductive electrodes, have been designed to enhance both stretchability and sensitivity. The deformable electrodes are typically made from conductive elastic composites with resistance changes in geometric dimensions or alterations in the local electrical percolation pathways. Novel durable materials based on textiles, cellulose, and biocarbon materials have been developed in applications of biocompatible and biodegradable pressure sensors [28]. Despite significant advancements in developing novel pressure sensors using artificial structures and conductive materials, the traditional approach has yet to fully overcome the trade-off between sensitivity and linearity in pressure sensors [29].

Electrode materials of flexible and stretchable electronics need to obtain high mechanical flexibility and optical transparency while maintaining electrical conductivity [30,31]. In response to these demands, researchers have concentrated on creating flexible functional materials to replace conventional rigid materials in electronic devices. Therefore, flexible electronic materials including metal wires or films, carbon nanomaterials, and conducting polymers have been investigated [32,33]. Among them, conductive polymers have recently received significant attention owing to their electrochemical and thermal stability, excellent electrical conductivity, and high transparency [34]. PEDOT:PSS is the most widely studied conducting polymer due to its high transparency in the visible spectrum, ease of solution processing, high work function, and significant mechanical stability [35]. However, since the pristine PEDOT film has a low conductivity of less than 1 S/cm, polar solvents of DMSO (dimethyl sulfoxide) and EG (ethylene glycol) are commonly used to enhance its electrical conductivity [36].

PDMS-based films with various surface and hierarchical microstructures have been developed for the use of pressure sensors [37]. The geometry and parameters of the microstructure have a significant influence on the contact area and local stress when pressure is applied. PDMS films with various microstructures including micropillar, micropyramid, and microdome arrays have been used to fabricate highly sensitive pressure sensors [38]. In general, pressure sensors with nano/microstructure patterns provide high sensitivity by significantly increasing the contact area under low-pressure conditions. However, as deformation progresses, the sensitivity of the pressure sensor greatly declines. Maintaining high sensitivity over a broad linear range is ideal for the best sensor performance [39,40]. An alternative approach to piezoresistive sensors is to produce PDMS microstructures with random pyramid architectures to enhance sensitivity by adjusting the height and spacing of the micropyramids [41]. Pressure sensors with irregular microstructures exhibit high sensitivity while maintaining broad linear sensing ranges [42,43]. When a small pressure is applied to the sensor, the contact area rapidly increases with the applied pressure due to the concentrated deformation of large microstructures, resulting in high sensitivity of the pressure sensor. As pressure increases, tiny microstructures contribute to electrical contacts, enabling pressure sensing over a wider linear range.

In the present study, we developed a low-cost pressure sensor with improved sensitivity and a fast response time by adding a PEDOT:PSS thin film to the surface of PDMS that had already been patterned with micropyramids of various heights. Cu-assisted chemical etching (CACE) was employed during the sensor fabrication process [44,45]. Etching times of 3, 5, and 10 min were also used with a silicon mold to produce micro-inverted pyramids with random heights. Previous microstructure-based pressure sensors were primarily manufactured using photolithography, 3D printing, and laser-assisted microengineering

techniques [46,47]. However, these methods are often costly and time consuming. In contrast, the CACE process can create highly accurate inverted pyramid shapes on silicon surfaces. As the etching proceeds, the CACE selectively removes specific crystal planes, allowing for precise control over the three dimensions of the structure. This method enables the formation of either randomly arranged micropylramids or uniformly patterned structures with varying depths. Additionally, the CACE method uses inexpensive chemicals and does not require complex machinery to produce high-quality nanostructures [44,45]. The properties of the PEDOT:PSS composite were confirmed using Raman spectroscopy. Several peaks representing the specific vibrational modes of PEDOT and PSS were identified in the composite. A resistive pressure sensor based on the PDMS/PEDOT:PSS bilayer structure with micropylramids of random heights was developed using the CACE process and demonstrated improved sensitivity, a rapid response time, and high repeatability.

## 2. Experimental Section

### 2.1. Materials and Reagents

PDMS (Sylgard 184, silicon elastomer) and a corresponding curing agent were purchased from Dow Corning Co., Ltd (Midland, MI, USA).  $\text{Cu}(\text{NO}_3)_2$ , hydrogen peroxide ( $\text{H}_2\text{O}_2$ , 30%, GR), sulfuric acid ( $\text{H}_2\text{SO}_4$ ), hydrogen fluoride (HF), toluene, and trichloro(1H,1H,2H,2H-perfluorooctyl)silane were purchased from Sigma Aldrich (Burlington, MA, USA). Si(100) wafers were purchased from Buyssemi, Korea. All materials were used directly without further purification unless otherwise noted.

### 2.2. Silicon Mold Fabrication

The silicon mold was created using CACE. First, the boron-doped (1–10  $\Omega\cdot\text{cm}$ ), 500  $\mu\text{m}$  thick, (100)-oriented, double-polished silicon wafers were thoroughly rinsed in acetone and deionized (DI) water for about 10 min to remove any organic contaminants. Wet etching of the silicon was then conducted using a Cu-based acid solution containing 5 mM  $\text{Cu}(\text{NO}_3)_2$ , 4.6 M HF, and 0.55 M  $\text{H}_2\text{O}_2$  at 50 °C. The etching times were 3, 5, and 10 min. The residual Cu nanoparticles were subsequently removed using a concentrated nitric acid ( $\text{HNO}_3$ ) solution in a sonication bath.

### 2.3. PEDOT:PSS Composite

To prepare the PEDOT:PSS composite, a pristine PEDOT:PSS solution was stirred at 200 rpm and 40 °C to obtain the desired volume at a 2 $\times$  concentration. Based on the weight of PEDOT:PSS, 10 wt.% of ethylene glycol (EG) and 1.5 wt.% of TX (Triton)-100 were added, and the solution was vortexed for 10 min at room temperature.

### 2.4. Pressure Sensor Fabrication

A piranha solution was prepared by slowly adding  $\text{H}_2\text{O}_2$  to concentrated  $\text{H}_2\text{SO}_4$  at a 3:1 ratio to control the exothermic reaction. The surface of the silicon mold was then soaked in the piranha solution for 30 min and rinsed with DI water. To facilitate the removal of the cured PDMS from the silicon mold without damaging the pattern, the surface of the silicon mold was coated with a self-assembling monolayer of trichloro(1H,1H,2H,2H-perfluorooctyl)silane (FOTS). The mold was placed in a sonication bath for 10 min and in a vacuum chamber for 60 min at room temperature. It was then annealed at 150 °C for 60 min. This process transformed the previously hydrophilic surface into a hydrophobic one.

The curing agent was mixed at a 10:1 ratio with the PDMS elastomer, and the mixture was cast onto the silicon mold. Oxygen ( $\text{O}_2$ ) and nitrogen ( $\text{N}_2$ ) contained in the mixture and residual air bubbles generated during mixing were extracted in a vacuum chamber to improve the quality of the mold by removing air bubbles inside the PDMS mixture. The PDMS was then cured at 70 °C for 4 h and peeled off the silicon mold. The pressure sensor was fabricated by casting the PEDOT:PSS composite onto the PDMS mold using spin coating (500 rpm for 20 s or 200 rpm for 60 s). The sensor was then annealed at 140 °C for 60 min.

### 2.5. Characterization and Measurements

The surface morphology of the silicon and PDMS molds was analyzed using a scanning electron microscope (SEM, Olympus OLS4500, Tokyo, Japan). Changes in the electrical resistance of the sensor due to changes in pressure were obtained using a source meter (Keithley 2400, Tektronix, Beaverton, OR, USA).

## 3. Results and Discussion

### 3.1. Preparation and Characterization

Figure 1 summarizes the operating principles of the proposed resistive pressure sensor based on a PEDOT:PSS thin film coating on microstructured PDMS with micropyramids of random heights. The sensing mechanism is a change in resistance when a constant pressure is applied to the upper surface of the sensor. As shown in Figure 1a, when a certain pressure is applied to the upper surface of the sensor, the change in resistance is measured. Figure 1b shows a side view of a pair of resistive pressure sensors based on the PDMS/PEDOT:PSS facing each other with electrodes connected to the top and bottom sensors. The total resistance of the sensor is determined by the resistance of the PDMS/PEDOT:PSS layer and the electrode. However, because the resistance of the electrode is fixed, the sensor's resistance signal is mainly determined by the PDMS/PEDOT:PSS layer, as illustrated in Equation (1).

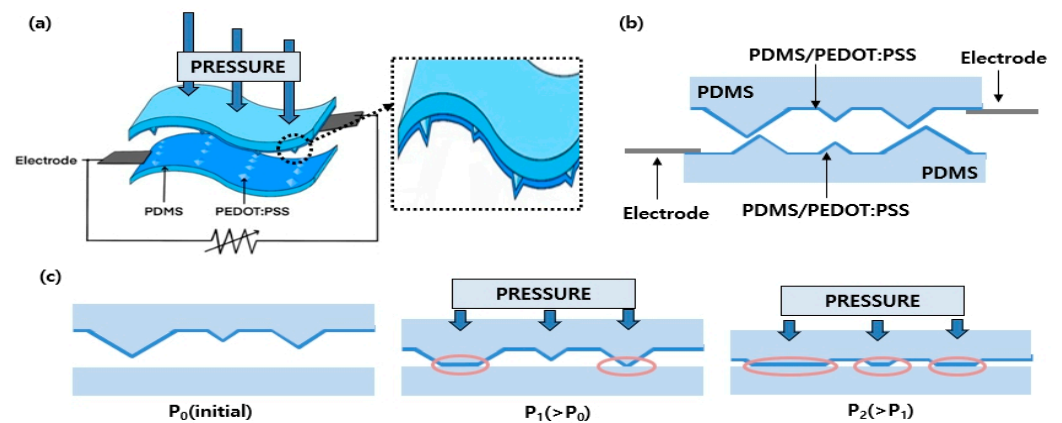


**Figure 1.** Operating principles for the proposed resistive pressure sensor based on a PEDOT:PSS thin film coating on microstructured PDMS with micropyramids of random height. (a) Mechanisms associated with the change in resistance when constant pressure is applied to the upper surface of the sensor. (b) Side view of a resistive pressure sensor based on a PEDOT:PSS thin film on PDMS with a micropyramid structure. (c) Morphological change in the sensor with a change in the sensor pressure.

Figure 1c shows the morphological changes in the sensor with a change in pressure from an initial pressure  $P_0$  to  $P_1$  and  $P_2$ . The sensitivity of the sensor is defined as

$$S = \frac{\Delta R/R_0}{\Delta P} \quad (2)$$

where  $R$  is the sensor's output resistance,  $\Delta P$  is the change in pressure, and  $R_0$  is the sensor's initial resistance. The change in resistance due to the change in pressure is expressed as  $\Delta R/R_0$ .

Figure 2 presents the fabrication process for the silicon and PDMS molds. Figure 2a shows the CACE process used to obtain an inverted pyramid structure via time-dependent etching. This selective etching is a proper method for creating pyramidal structures of random heights and has the advantage of processing large areas [44,45]. Copper nanoparticles (CuNPs) act as a catalyst to promote redox reactions on the silicon surface, and etching proceeds as HF removes the oxide film. First, copper ions ( $\text{Cu}^{2+}$ ) and hydrogen perox-

ide ( $\text{H}_2\text{O}_2$ ) react on the silicon surface to generate Cu nanoparticles ( $\text{CuNP}^*$ ) expressed as follows:

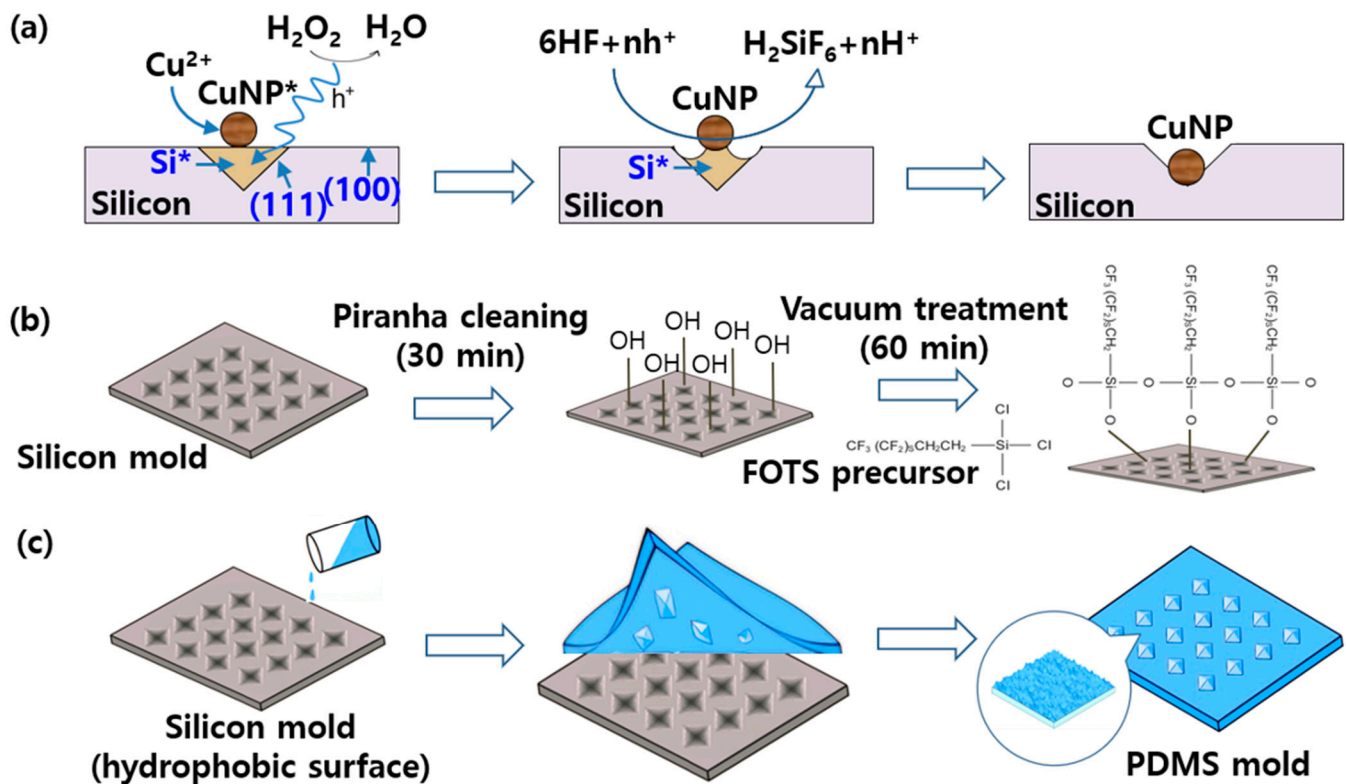
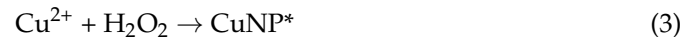
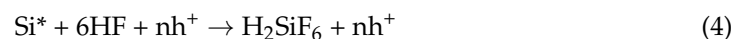


**Figure 2.** Fabrication process for the silicon and PDMS molds. (a) Time-dependent Cu-assisted chemical etching (CACE) to obtain an inverted pyramid structure. (b) Piranha cleaning process switches the surface of the silicon mold from hydrophobic to hydrophilic. (c) PDMS mold obtained from the hydrophobic silicon mold.

In this process, a part of the silicon (Si) surface is oxidized to  $\text{Si}^*$ , and  $\text{H}_2\text{O}_2$  decomposes into  $\text{H}_2\text{O}$  and  $\text{O}_2$ . Next, the formed  $\text{CuNPs}$  promote etching of the silicon surface. Here, an etchant of HF (hydrofluoric acid) is used to selectively remove a specific crystal plane (111) of the silicon as follows:



Here, the silicon is continuously etched by repeating this process. In the early stage of etching, the process proceeds isotropically, but as time passes, the concentration of hydrogen peroxide decreases, and the etching proceeds anisotropically due to the influence of copper.  $\text{CuNPs}$  continue to promote etching, but silicon is etched only in a specific direction, forming the desired structure. After etching, residual copper is removed through concentrated nitric acid treatment, and the etched silicon surface forms an inverted pyramid structure according to the crystal direction. The etching times were 3, 5, and 10 min. After a predetermined etching time, the silicon substrate was removed from the etching solution and immediately immersed in water to prevent further etching.

As illustrated in Figure 2b, the piranha cleaning process makes the surface of the silicon mold hydrophilic via surface functionalization with silanol groups ( $\text{Si-OH}$ ) during the oxidation process. For this reason, FOTS treatment was used to change the functionalized surface back to hydrophobic. Figure 2c shows the process of obtaining PDMS molds from the hydrophobic silicon molds.

Figure 3 presents SEM images of silicon and PDMS molds. Figure 3a shows the surface morphology of a (100) silicon wafer etched using 5 mM  $\text{Cu}(\text{NO}_3)_2$ , 4.6 M HF, and 0.55 M  $\text{H}_2\text{O}_2$ , with the residual Cu nanoparticles removed. The etching rate for silicon wafers differs depending on the crystallographic orientation of the substrate, generally decreasing in the order of  $(100) \approx (110) > (111)$ . As the etching time increased from 3 to 5 to 10 min, an inverted pyramid structure was observed in the silicon mold. Etching for 3 min led to a uniform distribution of inverted pyramids over the surface, with the enlarged image revealing sharp, defined features. With 5 min of etching, the inverted pyramids were cleaner, deeper, and square-shaped, with the enlarged image showing sharper edges and a greater depth. After etching for 10 min, the surface clarity disappeared, and the enlarged image showed an irregular surface.

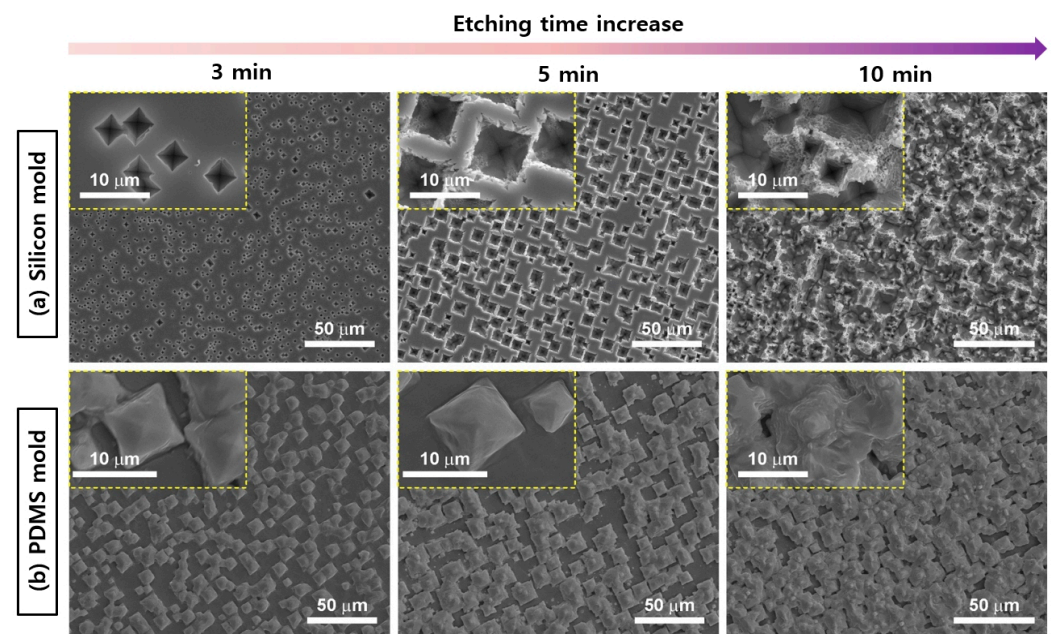


**Figure 3.** SEM images of silicon and PDMS molds. (a) SEM images of microstructures at a magnification of  $50\times$  on silicon molds etched for 3, 5, and 10 min in a mixture of 5 mM  $\text{Cu}(\text{NO}_3)_2$ , 4.6 M HF, and 0.55 M  $\text{H}_2\text{O}_2$  (inset: higher magnification view of the microstructures). (b) SEM image of microstructures at a magnification of  $50\times$  on the PDMS mold fabricated from the silicon mold in (a) etched for 3, 5, and 10 min (inset: higher magnification view of the microstructures).

Figure 3b presents SEM images of the pyramid structure of the PDMS mold obtained from the silicon mold. With 3 min of etching, uniformly arranged pyramids appeared on the surface, with the enlarged image revealing distinct individual block shapes. After 5 min of etching, a uniform distribution of more pronounced, deep square-shaped pyramids was observed, with the enlarged image showing well-formed block shapes. With an etching time of 10 min, the surface pattern became irregular, and individual pyramid shapes became indistinct.

Collectively, the SEM images demonstrated that the etching time had a significant effect on the surface morphology of the silicon and PDMS molds. The silicon mold tended to exhibit more distinct and sharp features than the PDMS mold. Based on the results, 5 min was selected as the optimal etching time for both molds to obtain well-defined surface features, and these molds were used in subsequent analyses.

### 3.2. Experimental Results

The fabrication process and Raman spectral characteristics of the proposed resistive pressure sensor based on PEDOT:PSS thin films and PDMS with micropylramid structures of random height are presented in Figure 4. The PEDOT:PSS was coated onto the PDMS

mold following the process outlined in Figure 4a, and Figure 4b displays the resulting resistive pressure sensor based on a PDMS/PEDOT:PSS, a pair of which are aligned to face each other and then connected to electrodes to produce the sensing device. The sensor was square, with a size of  $20 \times 20 \text{ mm}^2$ . Figure 4c presents the Raman scattering characteristics of the PEDOT:PSS composite. PEDOT is a conducting polymer, while PSS is nonconducting. Strong vibrations of the  $C\alpha = C\beta$  bonds are the primary characteristic of the PEDOT peaks, whereas PSS peaks are more prominent at lower Raman shifts. In the Raman spectrum for PEDOT:PSS, the peaks at  $1250 \text{ cm}^{-1}$ ,  $1365 \text{ cm}^{-1}$ ,  $1425 \text{ cm}^{-1}$ , and  $1550 \text{ cm}^{-1}$  are associated with vibrational modes of PEDOT, while the peaks at  $990 \text{ cm}^{-1}$  and  $1180 \text{ cm}^{-1}$  are characteristic of PSS. These distinct vibrational modes of PEDOT and PSS can be used to study the composition ratio, interactions, and structural changes within the composite.

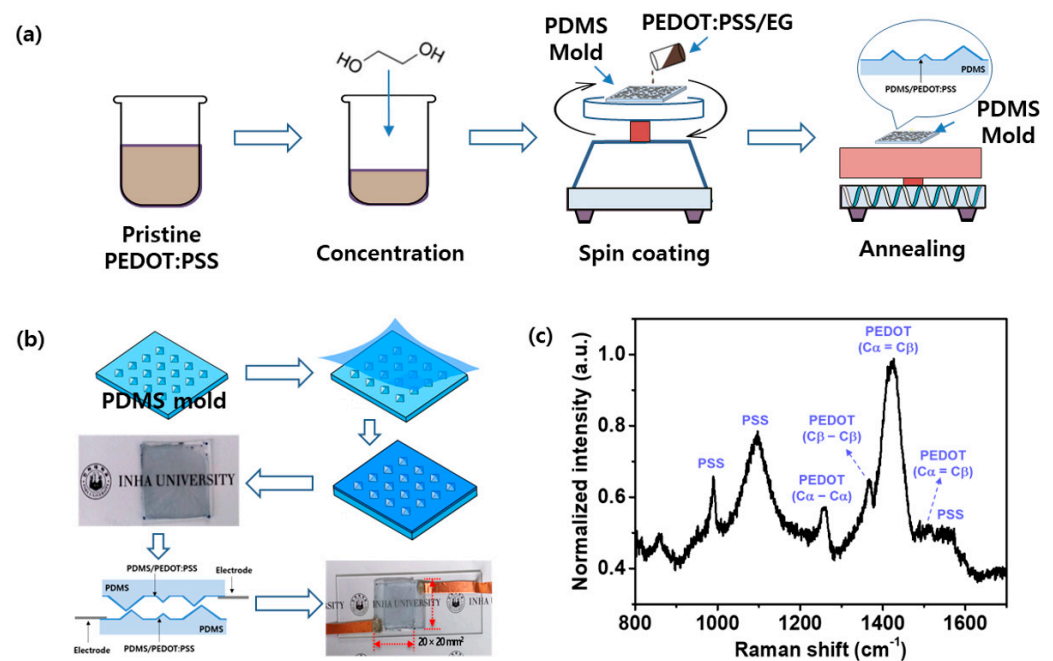


**Figure 4.** Fabrication process and Raman spectral characteristics of the PDMS/PEDOT:PSS-based resistive pressure sensor. (a) Coating of the PEDOT:PSS thin film on a PDMS mold. (b) Sensor device fabricated by attaching electrodes to PDMS/PEDOT:PSS sensors. (c) Raman scattering characteristics of the PEDOT:PSS composite.

Figure 5 shows the pressure sensitivity and response characteristics of the resistive pressure sensor based on PDMS coated with PEDOT:PSS with micropyramid structures of arbitrary height. Figure 5a shows a schematic diagram of the pressure measurement setup. The measurements were performed by placing precision weights corresponding to pressures in the range of 0.35 kPa to 2.58 kPa on the sensor surface, and the data were obtained using a Keithley 2400 source meter operated by the LabVIEW acquisition program.

Figure 5b shows the relative current changes ( $\Delta I/I_0$ ) when pressure loads are applied to the sensor. As the pressure increases, the relative current increases linearly from a measurement sensitivity of  $391 \text{ kPa}^{-1}$  to  $1.48 \text{ kPa}$ . The  $R^2$  value is 0.96, indicating a strong linear relationship between the pressure and current changes. The dynamic range of the sensor is 0.35 kPa to 2.58 kPa. The linear range of the sensor output responds linearly to the input pressure (0.3 to 1.48 kPa).

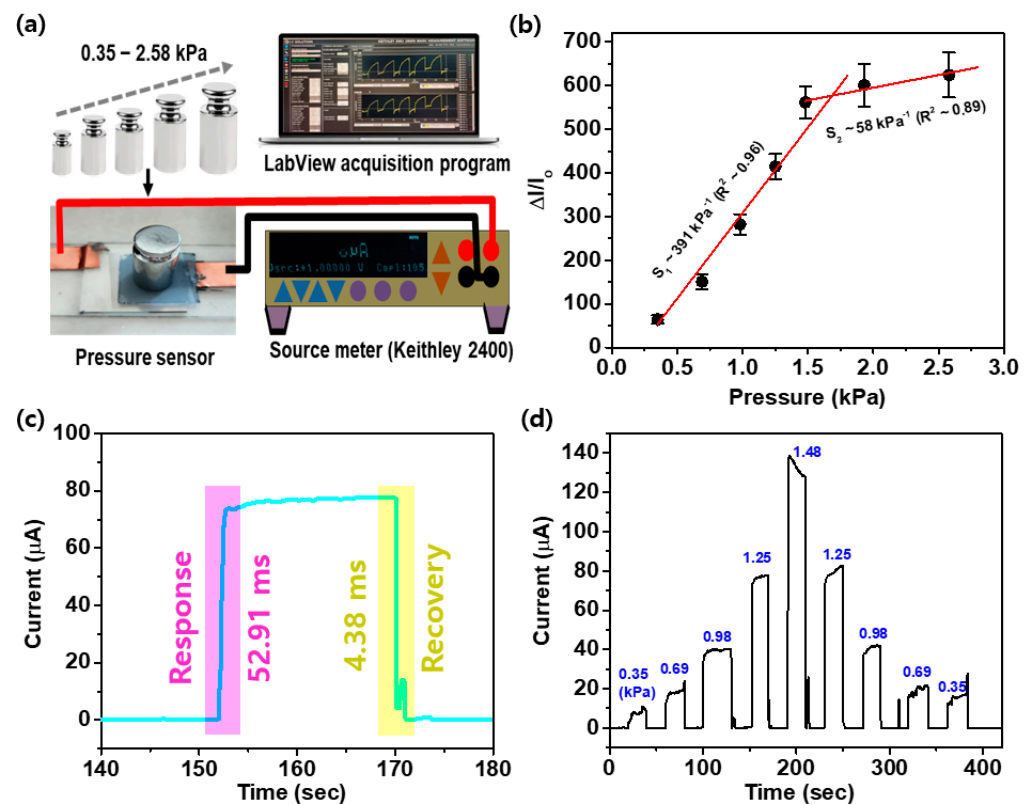


**Figure 5.** Pressure-sensing sensitivity and response characteristics of the proposed resistive pressure sensor based on PEDOT:PSS-coated PDMS with micropyramid structures of arbitrary heights. (a) Schematic of the pressure measurement setup. (b) Relative current changes ( $\Delta I/I_0$ ) according to different pressures (kPa) showing the dynamic range and linear range of the developed pressure sensor. (c) Response and recovery time. (d) Current response to changes in the pressure. Each peak represents the sensor's response to a change in pressure.

Figure 5c presents the response speed of the sensor in terms of the time required for the current to reach specific thresholds of 90% of the rise time (the signal rises from 10% to 90%) and 10% of the fall time (the signal falls from 90% to 10%). When an external load was applied, a rise time of 52.91 ms was observed. After reaching a consistent current with the load applied, the sensor's initial current was restored when the external load was removed. The observed fall time was 4.38 ms. These short rise and fall times demonstrate that the sensor can respond quickly.

Figure 5d displays the current response pattern according to changes in pressure for the sensor. The numbers in blue text represent the pressure in kPa that corresponds to the current response of each peak. The results highlight the repeatability of the sensor response when the load pressure is repeatedly increased and reduced from 0 to 1.48 kPa. As the pressure increased, the current also tended to increase. In practical sensor applications, sensitivity and response time are important metrics, and our proposed sensor demonstrates high sensitivity and a rapid response time.

Table 1 summarizes recent advances in pressure sensors based on typical performance parameters including materials, sensitivity, pressure ranges, and response time. The PDMS/PEDOT:PSS sensor developed in this study exhibits higher sensitivity ( $391 \text{ kPa}^{-1}$ ) than the other materials, especially in the low-pressure range (0 to 2.65 kPa). The PDMS/PEDOT:PSS sensor has a response time of 52.91 ms, which is comparable to some of the other sensors but faster than the MXene- and carbon nanostructure-based sensors and slower than the CNT/PDMS and aligned Ni/PDMS sensors.



**Table 1.** Several flexible piezoresistive pressure sensors reported in the literature.

| Materials                              | Sensitivity                       | Pressure Range | Response Time | Reference |
|----------------------------------------|-----------------------------------|----------------|---------------|-----------|
| MXene                                  | 148.26 kPa <sup>-1</sup>          | 0~16 kPa       | 120 ms        | [48]      |
| Urchin-like hollow carbon spheres      | 260.3 kPa <sup>-1</sup>           | 1~10,000 Pa    | 30/60 ms      | [49]      |
| CNT/PDMS                               | 15.1 kPa <sup>-1</sup>            | -              | 4 ms          | [50]      |
| Carbon nanostructure on patterned PDMS | 1.214 kPa <sup>-1</sup>           | 0~100 Pa       | 266/766 ms    | [51]      |
| Carbon nanofibers/PDMS                 | 0.60 kPa <sup>-1</sup>            | 0~1 kPa        | 30/25 ms      | [52]      |
| MXene on patterned PDMS                | 2.6 kPa <sup>-1</sup>             | 0~30 kPa       | 40/40 ms      | [53]      |
| Aligned Ni/PDMS                        | 0.72 kPa <sup>-1</sup> at 357 kPa | 373 kPa        | ~12/~20 ms    | [54]      |
| PDMS/PEDOT:PSS                         | 391 kPa <sup>-1</sup>             | 0.3~1.48 kPa   | 52.91 ms      | This work |

Figure 6 presents the cyclic loading/unloading test response characteristics of the resistive pressure sensor based on the developed PDMS with micropyramid structures of random height and a PEDOT:PSS coating. The response characteristics were measured using a source meter. The experiments used paired microstructured PDMS sensors (etching time = 5 min). To characterize the mechanical stability of the sensor, the device was continuously measured for approximately 150 cycles at a pressure of 1.25 kPa. Even after 150 cycles of measurement, the sensor maintained stable performance.

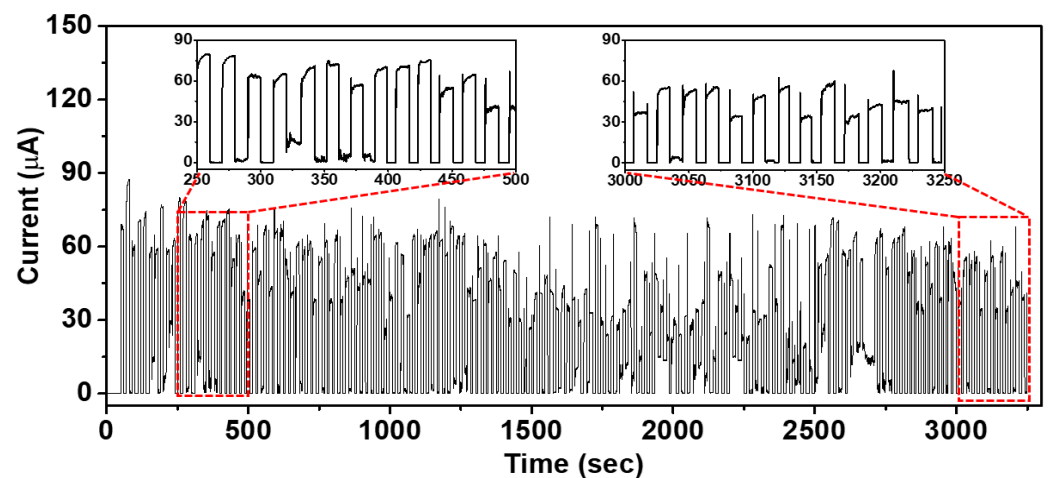


**Figure 6.** Current response of the proposed resistive pressure sensor based on microstructured PDMS/PEDOT:PSS when a pressure of 1.25 kPa is repeatedly loaded and unloaded for 150 cycles.

#### 4. Conclusions

In this study, we developed and demonstrated a resistive pressure sensor with enhanced sensitivity based on a PDMS/PEDOT:PSS bilayer structure with micropyramids of random heights. The originality of this research lies in the fabrication of micropyramid structures with random heights through the CACE process as well as an evaluation of electrical characteristics for the use of highly sensitive pressure sensors. The sensing mechanism was the change in resistance to pressure when constant pressure was applied to the upper surface of the sensor. The resistive pressure sensor was fabricated using a silicon mold that was etched with etching times of 3, 5, and 10 min, and this mold was used to produce the PDMS mold. The structure of these molds was investigated using SEM images, and the properties of the PEDOT:PSS composite were analyzed using Raman spectroscopy. A sensor device with a pair of microstructured PDMS sensors (etching time of 5 min) was used to test the pressure-sensing sensitivity and response characteristics of the fabricated

resistive pressure sensor device. The sensor characteristics were measured over a load range of 0 to 2.58 kPa. The sensitivity was  $391 \text{ kPa}^{-1}$  in the range of 0.3 to 1.48 kPa and the  $R^2$  value was 0.96, indicating a strong linear relationship between the pressure and current changes. The dynamic range of the sensor was 0.35 kPa to 2.58 kPa. The sensor's rise and fall times were 52.01 ms and 4.38 ms, respectively, representing a rapid response time. This newly developed resistive pressure sensor can be widely used in various applications including wearable electronic devices and electronic skin.

**Author Contributions:** Conceptualization, methodology, software, validation, formal analysis, investigation, writing, S.K., D.Y.K.; supervision, D.Y.K.; project administration, S.K., D.Y.K.; funding, D.Y.K. All authors have read and agreed to the published version of the manuscript.

**Funding:** This work was supported by an Inha University Research Grant.

**Data Availability Statement:** The data presented in this study are available on request from the corresponding author.

**Conflicts of Interest:** The authors declare no conflicts of interest.

## References

1. Wu, Y.; Chen, E.; Weng, X.; He, Z.; Chang, G.; Pan, X.; Liu, J.; Huang, K.; Huang, K.; Lei, M. Conductive polyvinyl alcohol/silver nanoparticles hydrogel sensor with large draw ratio, high sensitivity and high stability for human behavior monitoring. *Eng. Sci.* **2022**, *18*, 113–120. [[CrossRef](#)]
2. Gao, W.; Emaminejad, S.; Nyein, H.Y.; Challa, S.; Chen, K.; Peck, A.; Fahad, H.M.; Ota, H.; Shiraki, H.; Kiriya, D.; et al. Fully integrated wearable sensor arrays for multiplexed in situ perspiration analysis. *Nature* **2016**, *529*, 509–514. [[CrossRef](#)] [[PubMed](#)]
3. Mammock, M.L.; Chortos, A.; Tee, B.C.-K.; Tok, J.B.-H.; Bao, Z. 25th anniversary article: The evolution of electronic skin (E-Skin): A brief history, design considerations, and recent progress. *Adv. Mater.* **2013**, *25*, 5997–6038. [[CrossRef](#)]
4. Thuruthel, T.G.; Shih, B.; Laschi, C.; Tolley, M.T. Soft robot perception using embedded soft sensors and recurrent neural networks. *Science Robotics* **2019**, *4*, eaav1488. [[CrossRef](#)]
5. Ding, Y.; Yang, J.; Tolle, C.R.; Zhu, Z. Flexible and compressible PEDOT: PSS@ melamine conductive sponge prepared via one-step dip coating as piezoresistive pressure sensor for human motion detection. *ACS Appl. Mater. Interfaces* **2018**, *10*, 16077–16086. [[CrossRef](#)] [[PubMed](#)]
6. Liu, Z.; Li, G.; Qin, Q.; Mi, L.; Li, G.; Zheng, G.; Liu, C.; Li, Q.; Liu, X. Electrospun PVDF/PAN membrane for pressure sensor and sodium-ion battery separator. *Adv. Compos. Hybrid Mater.* **2021**, *4*, 1215–1225. [[CrossRef](#)]
7. Dos Santos, A.; Pinela, N.; Alves, P.; Santos, R.; Farinha, R.; Fortunato, E.; Martins, R.; Águas, H.; Igreja, R. E-skin bimodal sensors for robotics and prosthesis using PDMS molds engraved by laser. *Sensors* **2019**, *19*, 899. [[CrossRef](#)]
8. Zang, Y.; Zhang, F.; Di, C.A.; Zhu, D. Advances of flexible pressure sensors toward artificial intelligence and health care applications. *Mater. Horiz.* **2015**, *2*, 140–156. [[CrossRef](#)]
9. Chen, Z.; Yu, J.; Zhang, X.; Zeng, H.; Li, Y.; Wu, J.; Tao, K. A button switch inspired duplex hydrogel sensor based on both triboelectric and piezoresistive effects for detecting dynamic and static pressure. *Nanotechnol. Precis. Eng. (NPE)* **2022**, *5*, 023002. [[CrossRef](#)]
10. Li, S.; Zhang, Y.; Wang, Y.; Xia, K.; Yin, Z.; Wang, H.; Zhang, M.; Liang, X.; Lu, H.; Zhu, M.; et al. Physical sensors for skin-inspired electronics. *InfoMat* **2020**, *2*, 184–211. [[CrossRef](#)]
11. Zhang, L.; Zhang, S.; Wang, C.; Zhou, Q.; Zhang, H.; Pan, G.B. Highly sensitive capacitive flexible pressure sensor based on a high-permittivity MXene nanocomposite and 3D network electrode for wearable electronics. *ACS Sens.* **2021**, *6*, 2630–2641. [[CrossRef](#)] [[PubMed](#)]
12. Mo, L.; Meng, X.; Zhao, J.; Pan, Y.; Sun, Z.; Guo, Z.; Wang, W.; Peng, Z.; Shang, C.; Han, S.; et al. Full printed flexible pressure sensor based on microcapsule controllable structure and composite dielectrics. *Flex. Print. Electron.* **2021**, *6*, 014001. [[CrossRef](#)]
13. Ji, Z.; Zhang, M. Highly sensitive and stretchable piezoelectric strain sensor enabled wearable devices for real-time monitoring of respiratory and heartbeat simultaneously. *Nanotechnol. Precis. Eng. (NPE)* **2022**, *5*, 013002. [[CrossRef](#)]
14. Xie, W.; Yao, F.; Gu, H.; Du, A.; Lei, Q.; Naik, N.; Guo, Z. Magnetoresistive and piezoresistive polyaniline nanoarrays in-situ polymerized surrounding magnetic graphene aerogel. *Adv. Compos. Hybrid Mater.* **2022**, *5*, 1003–1016. [[CrossRef](#)]
15. Liu, Y.; Jiang, X.; Yang, H.; Qin, H.; Wang, W. Structural engineering in piezoresistive micropressure sensors: A focused review. *Micromachines* **2023**, *14*, 1507. [[CrossRef](#)] [[PubMed](#)]
16. Meng, Q.; Lu, Y.; Wang, J.; Chen, D.; Chen, J. A piezoresistive pressure sensor with optimized positions and thickness of piezoresistors. *Micromachines* **2021**, *12*, 1095. [[CrossRef](#)]
17. Yao, H.; Yu, Z.; Huang, F.; Pan, T.; Tang, C.; Zhang, H. A flexible piezoresistive pressure sensor comprising a microstructure printed with poly (3, 4-ethylenedioxythiophene): Poly (styrenesulfonate) copolymers@ graphene hybrid ink. *J. Mater. Chem. C* **2023**, *11*, 13324–13334. [[CrossRef](#)]

18. Wei, H.; Li, X.; Yao, F.; Feng, X.; Zhu, X. Flexible piezoresistive pressure sensor based on a graphene-carbon nanotube-polydimethylsiloxane composite. *Nanotechnol. Precis. Eng.* **2024**, *7*, 3. [[CrossRef](#)]
19. Wang, P.; Yu, W.; Li, G.; Meng, C.; Guo, S. Printable, flexible, breathable and sweatproof bifunctional sensors based on an all-nanofiber platform for fully decoupled pressure–temperature sensing application. *Chem. Eng. J.* **2023**, *4*, 139174. [[CrossRef](#)]
20. Yang, W.; Xie, M.; Zhang, X.; Sun, X.; Zhou, C.; Chang, Y.; Zhang, H.; Duan, X. Multifunctional soft robotic finger based on a nanoscale flexible temperature–pressure tactile sensor for material recognition. *ACS Appl. Mater. Interfaces* **2021**, *13*, 55756–55765. [[CrossRef](#)]
21. Duan, Y.; He, S.; Wu, J.; Su, B.; Wang, Y. Recent progress in flexible pressure sensor arrays. *Nanomaterials* **2022**, *12*, 2495. [[CrossRef](#)] [[PubMed](#)]
22. Pyo, S.; Lee, J.; Bae, K.; Sim, S.; Kim, J. Recent progress in flexible tactile sensors for human-interactive systems: From sensors to advanced applications. *Adv. Mater.* **2021**, *33*, 2005902. [[CrossRef](#)]
23. Cheng, L.; Wang, R.; Hao, X.; Liu, G. Design of flexible pressure sensor based on conical microstructure PDMS-bilayer graphene. *Sensors* **2021**, *21*, 289. [[CrossRef](#)] [[PubMed](#)]
24. Deng, C.; Zhao, S.; Su, E.; Li, Y.; Wu, F. Trilayer MXene fabric for integrated ultrasensitive pressure sensor and wearable heater. *Adv. Mater. Technol.* **2021**, *6*, 2100574. [[CrossRef](#)]
25. Kim, J.; Park, D.; Moon, S.; Park, C.; Thiyagarajan, K.; Choi, S.; Hwang, H.; Jeong, U. Omnidirectional tactile profiling using a deformable pressure sensor array based on localized piezoresistivity. *Adv. Mater. Technol.* **2022**, *7*, 2100688. [[CrossRef](#)]
26. Hung, L.S.; Chen, C.H. Materials science and engineering: R: Reports. *Mater. Sci. Eng.* **2002**, *39*, 143–222. [[CrossRef](#)]
27. Zhao, Y.; Liu, L.; Li, Z.; Wang, F.; Chen, X.; Liu, J.; Song, C.; Yao, J. Facile fabrication of highly sensitive and durable cotton fabric-based pressure sensors for motion and pulse monitoring. *J. Mater. Chem. C* **2021**, *9*, 12605–12614. [[CrossRef](#)]
28. Pan, H.; Lee, T.-W. Recent progress in development of wearable pressure sensors derived from biological materials. *Adv. Healthc. Mater.* **2021**, *10*, 2100460. [[CrossRef](#)]
29. Huang, L.; Zeng, R.; Tang, D.; Cao, X. Bioinspired and multiscale hierarchical design of a pressure sensor with high sensitivity and wide linearity range for high-throughput biodetection. *Nano Energy* **2022**, *99*, 107376. [[CrossRef](#)]
30. Yang, Y.; Deng, H.; Fu, Q. Recent progress on PEDOT: PSS based polymer blends and composites for flexible electronics and thermoelectric devices. *Mater. Chem. Front.* **2020**, *4*, 3130–3152. [[CrossRef](#)]
31. Fan, X.; Nie, W.; Tsai, H.; Wang, N.; Huang, H.; Cheng, Y.; Wen, R.; Ma, L.; Yan, F.; Xia, Y. PEDOT: PSS for flexible and stretchable electronics: Modifications, strategies, and applications. *Adv. Sci.* **2019**, *6*, 1900813. [[CrossRef](#)] [[PubMed](#)]
32. Liu, K.; Duan, T.; Zhang, F.; Tian, X.; Li, H.; Feng, M.; Wang, R.; Jiang, B.; Zhang, K. Flexible electrode materials for emerging electronics: Materials, fabrication and applications. *J. Mater. Chem. A* **2024**, *12*, 20606–20637. [[CrossRef](#)]
33. Tringides, C.M.; Vachicouras, N.; de Lázaro, I.; Wang, H.; Trouillet, A.; Seo, B.R.; Elosegui-Artola, A.; Fallegger, F.; Shin, Y.; Casiraghi, C.; et al. Viscoelastic surface electrode arrays to interface with viscoelastic tissues. *Nat. Nanotechnol.* **2021**, *16*, 1019–1029. [[CrossRef](#)] [[PubMed](#)]
34. Diez-Pascual, A.M.; Rahdar, A. Graphene-based polymer composites for flexible electronic applications. *Micromachines* **2022**, *13*, 1123. [[CrossRef](#)] [[PubMed](#)]
35. Lin, Y.-J.; Ni, W.-S.; Lee, J.-Y. Effect of incorporation of ethylene glycol into PEDOT: PSS on electron phonon coupling and conductivity. *J. Appl. Phys.* **2015**, *118*, 219901. [[CrossRef](#)]
36. Dong, J.; Portale, G. Role of the Processing Solvent on the Electrical Conductivity of PEDOT: PSS. *Adv. Mater. Interfaces* **2020**, *7*, 2000641. [[CrossRef](#)]
37. Singh, L.; Tripathy, K.; Bhattacharjee, M. Porous microstructure-assisted flexible and highly sensitive polymer piezoresistive pressure sensor. *Adv. Eng. Mater.* **2022**, *24*, 2200500. [[CrossRef](#)]
38. Tang, R.; Lu, F.; Liu, L.; Yan, Y.; Du, Q.; Zhang, B.; Zhou, T.; Fu, H. Flexible pressure sensors with microstructures. *Nano Sel.* **2021**, *2*, 1874–1901. [[CrossRef](#)]
39. Pang, Y.; Zhang, K.; Yang, Z.; Jiang, S.; Ju, Z.; Li, Y.; Wang, X.; Wang, D.; Jian, M.; Zhang, Y.; et al. Epidermis microstructure inspired graphene pressure sensor with random distributed spinosum for high sensitivity and large linearity. *ACS Nano* **2018**, *12*, 2346–2354. [[CrossRef](#)]
40. Tu, S.; Xi, Y.; Cui, X.; Xu, Z.; Liu, Z.; Zhu, Y. Skin-inspired interlocked microstructures with soft-hard synergistic effect for high-sensitivity and wide-linear-range pressure sensing. *Chem. Eng. J.* **2024**, *496*, 154083. [[CrossRef](#)]
41. Zhao, Y.; Shen, T.; Zhang, M.; Yin, R.; Zheng, Y.; Liu, H.; Sun, H.; Liu, C.; Shen, C. Advancing the pressure sensing performance of conductive CNT/PDMS composite film by constructing a hierarchical-structured surface. *Nano Mater. Sci.* **2022**, *5*, 343–350. [[CrossRef](#)]
42. Jung, Y.; Choi, J.; Lee, W.; Ko, J.S.; Park, I.; Cho, H. Irregular microdome structure-based sensitive pressure sensor using internal popping of microspheres. *Adv. Funct. Mater.* **2022**, *32*, 2201147. [[CrossRef](#)]
43. Wang, Z.; Wang, S.; Zeng, J.; Ren, X.; Chee, A.J.; Yiu, B.Y.; Chung, W.C.; Yang, Y.; Yu, A.C.; Roberts, R.C.; et al. High sensitivity, wearable, piezoresistive pressure sensors based on irregular microhump structures and its applications in body motion sensing. *Small* **2016**, *12*, 3827–3836. [[CrossRef](#)] [[PubMed](#)]
44. Chen, W.; Liu, Y.; Yang, L.; Wu, J.; Chen, Q.; Zhao, Y.; Wang, Y.; Du, X. Difference in anisotropic etching characteristics of alkaline and copper based acid solutions for single-crystalline Si. *Sci. Rep.* **2018**, *8*, 3408. [[CrossRef](#)] [[PubMed](#)]

45. Zhao, S.; Yuan, G.; Wang, Q.; Liu, W.; Zhang, S.; Liu, Z.; Wang, J.; Li, J. Morphology control of c-Si via facile copper-assisted chemical etching: Managements on etch end-points. *Appl. Surf. Sci.* **2019**, *489*, 776–785. [[CrossRef](#)]
46. Huang, H.; Zhong, J.; Ye, Y.; Wu, R.; Luo, B.; Ning, H.; Qiu, T.; Luo, D.; Yao, R.; Peng, J. Research progresses in microstructure designs of flexible pressure sensors. *Polymers* **2022**, *14*, 3670. [[CrossRef](#)]
47. Gao, Y.; Xiao, T.; Li, Q.; Chen, Y.; Qiu, X.; Liu, J.; Bian, Y.; Xuan, F. Flexible microstructured pressure sensors: Design, fabrication and applications. *Nanotechnology* **2022**, *33*, 322002. [[CrossRef](#)]
48. Yan, J.; Ma, Y.; Li, X.; Zhang, C.; Cao, M.; Chen, W.; Luo, S.; Zhu, M.; Gao, Y. Flexible and high-sensitivity piezoresistive sensor based on MXene composite with wrinkle structure. *Ceram. Int.* **2020**, *46*, 23592–23598. [[CrossRef](#)]
49. Shi, L.; Li, Z.; Chen, M.; Qin, Y.; Jiang, Y.; Wu, L. Quantum effect-based flexible and transparent pressure sensors with ultrahigh sensitivity and sensing density. *Nat. Commun.* **2020**, *11*, 3529. [[CrossRef](#)]
50. Chen, W.; Yan, X. Progress in achieving high-performance piezoresistive and capacitive flexible pressure sensors: A review. *J. Mater. Sci. Technol.* **2020**, *43*, 175–188. [[CrossRef](#)]
51. Li, W.-D.; Pu, J.H.; Zhao, X.; Jia, J.; Ke, K.; Bao, R.Y.; Liu, Z.Y.; Yang, M.B.; Yang, W. Scalable fabrication of flexible piezoresistive pressure sensors based on occluded micro-structures for subtle pressure and force waveform detection. *J. Mater. Chem. C* **2020**, *8*, 16774–16783. [[CrossRef](#)]
52. Dai, S.-W.; Gu, Y.-L.; Zhao, L.; Zhang, W.; Gao, C.-H.; Wu, Y.-X.; Shen, S.-C.; Zhang, C.; Kong, T.-T.; Li, Y.-T.; et al. Bam-boo-Inspired Mechanically Flexible and Electrically Conductive Polydimethylsiloxane Foam Materials with Designed Hierarchical Pore Structures for Ultra-Sensitive and Reliable Piezoresistive Pressure Sensor. *Compos. Part B. Eng.* **2021**, *225*, 109243. [[CrossRef](#)]
53. Chen, B.; Zhang, L.; Li, H.; Lai, X.; Zeng, X. Skin-Inspired Flexible and High-Performance MXene@polydimethylsiloxane Piezoresistive Pressure Sensor for Human Motion Detection. *J. Colloid Interface Sci.* **2022**, *617*, 478–488. [[CrossRef](#)] [[PubMed](#)]
54. Kim, H.; Choi, S.; Lee, B.; Seo, J.; Lee, S.; Yoon, J.; Hong, Y. Nonpatterned Soft Piezoresistive Films with Filamentous Conduction Paths for Mimicking Multiple-Resolution Receptors of Human Skin. *ACS Appl. Mater. Interfaces* **2022**, *14*, 55088–55097. [[CrossRef](#)] [[PubMed](#)]

**Disclaimer/Publisher’s Note:** The statements, opinions and data contained in all publications are solely those of the individual author(s) and contributor(s) and not of MDPI and/or the editor(s). MDPI and/or the editor(s) disclaim responsibility for any injury to people or property resulting from any ideas, methods, instructions or products referred to in the content.